COVER SHEET

NOTE: This coversheet is intended for you to list your article title and author(s) name only —this page will not appear on the CD-ROM.

Paper Number: **1825**

Composite Cure Process Modeling and Simulations using COMPRO® and Validation of Residual Strains using Fiber Optics Sensors

Thammaiah Sreekantamurthy, Tyler B. Hudson, Tan-Hung Hou, Brian W. Grimsley

(FIRST PAGE OF ARTICLE – *align this to the top of page – leave space blank above ABSTRACT*)[1]

ABSTRACT

Composite cure process induced residual strains and warping deformations in composite components present significant challenges in the manufacturing of advanced composite structure. As a part of the Manufacturing Process and Simulation initiative of the NASA Advanced Composite Project (ACP), research is being conducted on the composite cure process by developing an understanding of the fundamental mechanisms by which the process induced factors influence the residual responses. In this regard, analytical studies have been conducted on the cure process modeling of composite structural parts with varied physical, thermal, and resin flow process characteristics. The cure process simulation results were analyzed to interpret the cure response predictions based on the underlying physics incorporated into the modeling tool. In the cure-kinetic analysis, the model predictions on the degree of cure, resin viscosity and modulus were interpreted with reference to the temperature distribution in the composite panel part and tool setup during autoclave or hot-press curing cycles. In the fiber-bed compaction simulation, the pore pressure and resin flow velocity in the porous media models, and the compaction strain responses under applied pressure were studied to interpret the fiber volume fraction distribution predictions. In the structural simulation, the effect of temperature on the resin and ply modulus, and thermal coefficient changes during curing on predicted mechanical strains and chemical cure shrinkage strains were studied to understand the residual strains and stress response predictions. In addition to computational analysis, experimental studies were conducted to measure strains during the curing of laminated panels by means of optical fiber Bragg grating sensors (FBGs) embedded in the resin impregnated panels. The residual strain measurements from laboratory tests were then compared with the analytical model predictions. The paper describes the cure process procedures and residual strain predications, and discusses pertinent experimental results from the validation studies.

[1] Thammaiah Sreekantamurthy, Analytical Mechanics Associates, Mail Stop 226, NASA Langley Research Center, Hampton, VA, 23681-2199.
[2] Tyler B. Hudson, National Institute of Aerospace, Mail Stop 226, NASA Langley Research Center, Hampton, VA, 23681-2199.
[3] Tan-Hung Hou, Mail Stop 226, NASA Langley Research Center, Hampton, VA, 23681-2199.
[4] Brian W. Grimsley, Mail Stop 226, NASA Langley Research Center, Hampton, VA, 23681-2199.

INTRODUCTION

Composite cure process induced residual strains and warping defects present significant challenges in the manufacturing of advanced composite structural components. Lack of effective means for overcoming these defects has resulted in ad-hoc and time-consuming trial and error approaches to alter the cure process during the manufacturing phase. Hence, better approaches have been sought to overcome residual strains and warping defects. However, a multitude of complex physical phenomena occurring in the composite cure process has hindered a better understanding of the formation of the cure induced defects. Composite cure process modeling and simulation methods have come a long way in recent years to enable analytical evaluation of the curing process. Cure process simulation software is becoming available to assess the curing responses from simulations of the physics of curing phenomenon such as cure kinetics, fiber-bed compaction, warping deformations and residual strains. In parallel development, real-time measurement and monitoring of cure state through the use of thermo-couples, fiber-optics, acoustics, dielectric, and other in-situ sensors have provided opportunities to measure the physical state of resin, and thus providing a better understanding of the curing phenomenon. As a part of the Manufacturing Process and Simulation initiative of the NASA Advanced Composite Project (ACP), research is being conducted on the composite cure process by developing an understanding of the basic mechanisms by which the process induced factors influence the residual responses.

The primary focus of this study was to develop cure process models of composite parts using commercial-off-the-shelf software to analyze and understand the cure responses with reference to the known physics of the composite curing process, and to compare the residual strain predictions from the analysis with those measured using fiber optics strain sensors in the laboratory. In this regard, analytical studies were conducted on the cure process modeling of composite structural parts such as composite flat panel, angle section, and corner-section components using commercial software COMPRO® and RAVEN® from Convergent Manufacturing Technology, Vancouver, Canada. This paper is focused on the cure process modeling and analysis of laminated panels. The studies involved thermo-kinetic, resin flow compaction, and residual strain analysis of the curing part. Experimental tests were conducted to measure strains during the curing of laminates by means of optical fiber strain sensing techniques. The paper first describes the material characteristics of the Hexcel® 8552 resin, followed by analysis of two- and three-dimensional cure models of laminates. The paper then describes the laminate fabrication with embedded optical strain sensors for residual strain measurements. Finally, the strains measured in the experimental tests are compared with those from the cure process analysis, and the results are summarized with concluding remarks.

AN UNDERSTANDING OF THE PHYSICS OF CURE MECHANICS

The earliest attempts to understand the mechanics of composite cure processes began in early ‘80s soon after mechanics of composite materials became well developed and widely modeled for simulation of structural responses. Many research articles have been published since then on the cure process of composites. References [1-6] describe

and discuss key concepts in the curing of epoxy matrix, thermo-chemical phenomenon including heat of reaction, viscosity, resin flow, residual stress and strain formation in the fiber-reinforced composites. Reference [3] states that although residual stress effects on structural integrity have been modeled and analyzed, the process of residual stress development during cure processing has not been well understood. Reference [4] explored many facets of the complex curing phenomenon to develop an understanding for advancement of the state-of-the-art. More recently, Johnston [7] and Hubert [8] focused on implementation of models of the curing mechanics incorporating material cure characteristics so that these cure processes can be simulated using structural analysis software MSC/NASTRAN®. An architecture of a cure process simulation software called COMPRO® for modeling the composite cure process has been implemented as described in references [9, 10] and the software operates on a database of material cure characteristics, and utilizes sophisticated finite element software ABAQUS® [11].

HEXCEL® IM7-8552 MATERIAL CHARACTERISTICS

Hexcel® IM7-8552 material was used in the fabrication and subsequent analysis of the laminated panel cure process. The basic material characteristics for the open source resin material Hexcel® 8552 at material points were derived from the RAVEN® material database and plotted in Figure 1. The figure shows the degree of cure and viscosity properties of the material for the nominal two stage cure temperature cycle recommended by the manufacturer. It is seen that the degree of cure of 0.8 is reached for the material, which is typical for the material. Initial drop in the viscosity signifies resin softening and flow in the prepreg material to allow for fiber-bed saturation and excess resin bleed. In the absence of complex viscosity data, the gelation point is interpreted to occur at a time point where the viscosity increases abruptly, after the minimum viscosity has been reached. For this material, the gelation time point is around 130 minutes into the cure. The glass transition temperature, T_g, was computed using the Benedetto's empirical formula [10]. The gelation point and vitrification point (T_g = T in the material) marks the phase transition of the material. An understanding of where these transition points occur is critical for the curing cycle development. The other significant material characteristics that affect the formation of residual strains are resin modulus, thermal expansion coefficients, and Poisson's ratios. These resin cure characteristics defined in RAVEN for a material point are extended to modeling of finite dimensional laminate, by modeling ply properties as a function of pure resin characteristics.

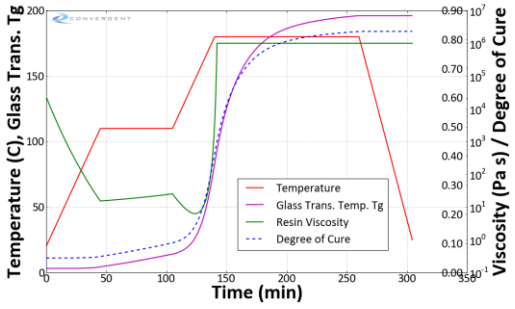

Figure 1: Basic material characteristics of Hexcel® 8552.

CURE PROCESS MODELING AND ANALYSIS SIMULATIONS

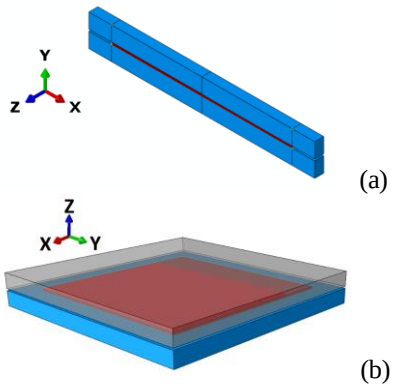

Figure 2: (a) Two-dimensional (2D), and (b) three-dimensional (3D) models of the panel cure process showing the prepreg layup in tooling assembly.

Cure process modeling and analysis of laminated composite panels were performed on two- and three-dimensional (3D) laminates to understand the responses beyond the material point. Analytical models of the cure kinetics, resin chemical shrinkage, fiber-bed compaction and resin flow in porous medium, deformation and strain mechanics were studied in reference to the physics of the laminate cure process. Model parameters having significant influence on the laminate cure responses were identified. Parameters included temperature and pressure gradients, heat flow, degree of cure and rate of cure, resin viscosity, permeability, resin modulus, fiber volume fraction, thermal expansion coefficient, orientation, and number of plies. A vacuum hot-press was chosen for the laminate curing process, which facilitated fiber-optics strain sensor wires passage into the hot-press chamber. The recommended cure cycle temperature and pressure in the hot-press were the same as for an autoclave.

Detailed studies were performed using two- and three-dimensional cure process models of laminated panels, which were based on the finite element models of the composite laminates, and the Hexcel® 8552 material cure characteristics. Analytical models of the selected laboratory test cases of square panels made of Hexcel® IM7-8552 prepreg sheets of size 30.5 cm x 30.5 cm (12 inch x 12 inch) were setup using COMPRO® and ABAQUS® software tools, so that simulations results from the analysis can be compared with residual strain and warping response measurements during the cure process. Cure process analysis simulations required through-the-thickness modeling to capture the thermal heat transfer, fiber-bed compaction, and stress and strains in the material using solid finite elements. The finite element models were developed using four layers of solid hexagonal elements across the thickness of the panel. The composite prepreg consisting of uniaxial, and cross-ply laminates with $[0_{12}/90_{12}]$ and $[+45_{12}/-45_{12}]$ layups were analyzed. The first set of cure process analyses were performed using a plain strain two-dimensional (2D) model of the panel (Figure 2a). Although, the 2D model served to approximate the through-the-thickness responses, a full 3D model of the laminate panels was required to capture the cure response distribution across the panel surface (Figure 2b). However, the 2D plain strain cure process model having much less number of solid 3D elements across the thickness is computationally less intensive than the 3D cure process model of the full panel. The 3D model consisted of about 3000 solid elements and included a tooling assembly consisting of top and bottom caul plates for the hot-press cure. Cure process response computations involved sequential uncoupled analysis using the thermo-chemical model, flow-compaction model, and residual stress and deformation models. Here, flow-compaction and structural analysis were based on the pre-determined temperature distribution in the part. Smeared layup properties were used for the heat transfer analysis as well as for fluid flow analysis employing the porous solid elements of ABAQUS®, whereas the structural analysis accommodated composite ply properties.

Transient heat transfer simulation established the temperature responses during the cure cycle over the surface as well as through-the-thickness of the panel model. The degree of cure, viscosity response, and resin modulus variation during the curing cycle were computed using the cure-kinetic models of Hexcel® 8552 resin. Selected heat-transfer boundary conditions on the tooling surfaces allowed for heat conduction into the prepreg material. The nonlinear friction contact surface interactions between the contact surfaces of the prepreg material and the surfaces of the steel caul plate tooling assembly were modeled in ABAQUS® with hard penalty constraints for "make or break" in the contact mechanisms defined to operate within the shear stress limits of the contact. Necessary boundary conditions were setup in the finite element models of the prepreg and tooling assembly of the panel. The flow-compaction simulation was performed to carry out the resin bleed and fiber-bed compaction in order to predict fiber volume fraction distribution in the consolidated prepreg part, and to predict the thickness of the laminate. The compaction model included specification of resin bleed surfaces, which were the two short side edge surfaces of the 2D model, and were the four side edge surfaces in the case of the 3D model. These models included the applied compaction pressure load during the cure cycle. The structural deformation and stress simulation included explicit composite layer definition of the part to simulate the formation of residual stresses and strains during the cure cycle, and included the temperature distribution to be applied during the cycle, which was determined in the previous simulation step of the heat transfer analysis. The analysis included "Tool-removal / Model change" interaction conditions of ABAQUS® to simulate tool removal to get the final residual stress, strain, and warping deformation of the consolidated panel.

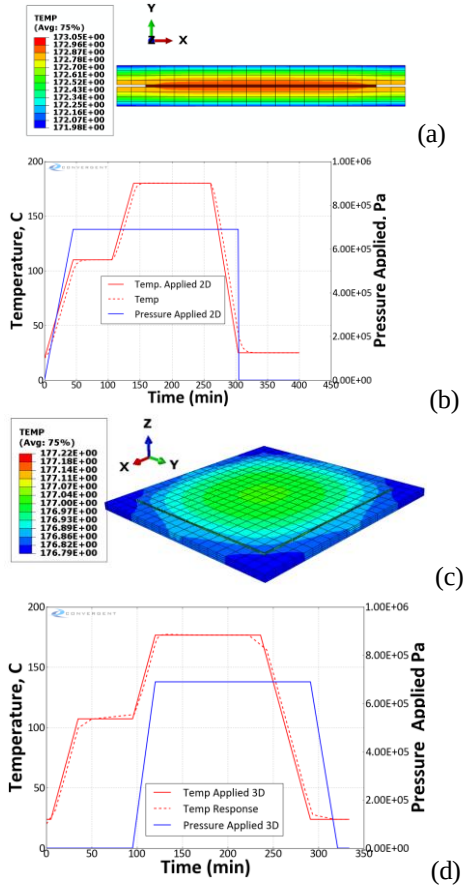

Figure 3: Temperature distribution - (a) on the cross-section of 2D model, (b) during cure cycle of 2D model, (c) on the surface of 3D model, (d) during cure cycle of 3D model.

Heat Transfer Simulation Results on Temperature Distribution

The applied temperature and pressure cure cycles for the 2D and 3D analysis models are shown in Figure 3. The Figures 3b and 3d show the temperature responses during the various stages of the heating and cooling cycles. The distribution of temperature responses over the thickness and across the cross-section of the 2D part at a selected time point in the cure cycle is shown in Figure 3a. The distribution of temperature over the surface of the 3D part is shown in Figure 3c. These temperature responses are a result of the transient heat transfer under applied heat flux in the tooling assembly. The

temperature response of the thin prepreg laminate essentially followed the applied temperature (Figure 3), with little exothermic overshoots and little temperature gradient over the part and tooling assembly. There were some basic differences in the modeling of the 2D and 3D analyses regarding the applied temperature, applied pressure, and incremental time-step inputs. Therefore, the temperature responses from these analyses were different over the cure cycle as plotted in Figure 4. The degree of cure and viscosity responses computed for these models for an element located at the center of the panel are shown in the figure. These responses were similar to the basic cure characteristics at a material point. Minor variation of viscosity over the surface existed at any given point in the cure, but significant variation occurred between consecutive time points of cure. The spatial and temporal distribution in the temperature responses were used in the uncoupled flow-compaction analysis, to estimate the fiber volume fraction, compaction strains, and compaction thickness of the part. The cure shrinkage strain responses that occur due to chemical reactions will be discussed later along with other thermal strains. The cure shrinkage strain, compaction strains, thermal strains, and formed the total strain occurring during the cure cycle.

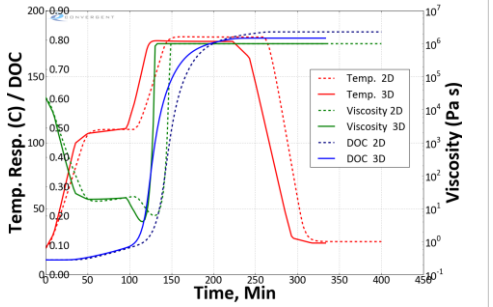

Figure 4: Degree of cure and viscosity at the center of panel from the 2D and 3D analysis.

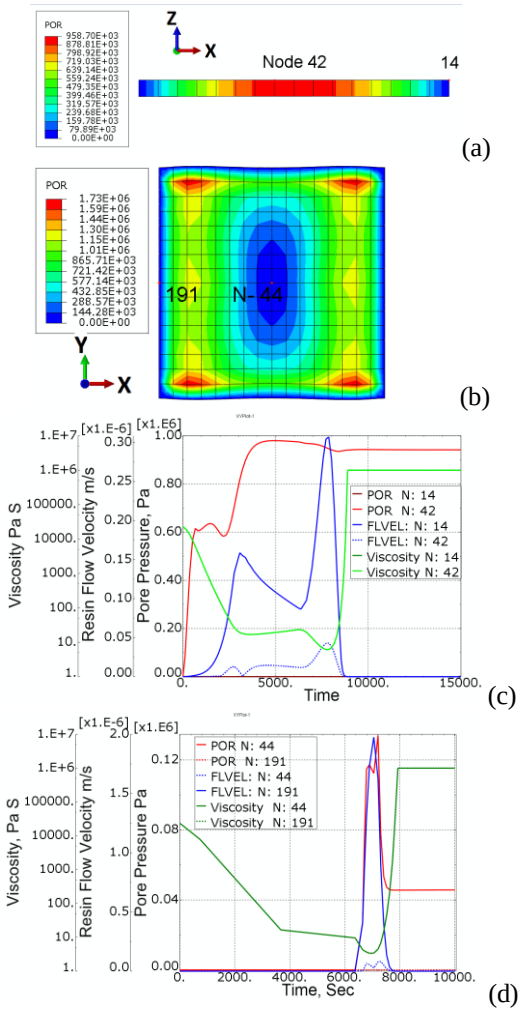

Figure 5: Pore pressure distribution over the surface of the (a) 2D model, (b) 3D model; and Viscosity, flow velocity, pore pressure during cure cycle of the (c) 2D, (d) 3D model of panel.

Flow-Compaction Analysis Results on Fiber Volume Fraction and Laminate Thickness

With known temperature distributions from the thermal-chemical analysis, the fiber volume fractions and final compaction thickness of the laminate were determined from the flow-compaction analysis simulation. The resin flow in the porous fiber-bed media was modeled with porous elements that incorporated pore pressure as a solution variable. As the part temperature increased, the resin viscosity drops, and the prepreg fiber-bed containing resin begins to expand in volume, developing pore pressure within the porous media. The resin bleed

during the cure cycle can be inferred from the plot of resin flow velocity and pore pressure (Figure 5b and 5d). Pore pressure distribution from the 2D and 3D models after the second temperature ramp are shown in Figures 5a and 5c where nearly zero pressure is indicated at the bleed edges of the panel. With rise in temperature and a decrease in viscosity, the resin begins to bleed out of the part, through the specified bleed edge boundary surfaces. From the viscosity, resin flow velocity, and pore pressure trends, the velocity and pore pressure have an inverse relationship with the viscosity. These responses follow Darcy's Law, which relate velocity, pressure gradient, and viscosity to the permeability of the porous medium. The fiber volume fraction distributions computed from the 2D and 3D models, after compaction are plotted in the Figures 6a and 6b. The results show that the fiber volume fraction distribution was higher around the bleed edge surfaces, however, the magnitude of this variation was small. Fiber volume fraction variation during the cure cycle is plotted in Figure 6c. The fiber-bed compaction continued while the resin is in the fluid or rubbery state, and stopped at the onset of gelation when resin viscosity became high. The variation of the mechanical properties from the prepreg state, to highly viscous or elastomeric state, and finally the vitreous or solid state are captured in Figure 7a. The elastomeric state of the material is indicated by the plot of the ratio of the bulk modulus to shear modulus of the material and is about 3000 (Figure 7) and from Poisson's ratio which changed from 0.5, as the material is viscous and incompressible, to 0.37 as the material transformed to a solid state. At this stage, the resin modulus also increases significantly (Figure 7a). The fiber-bed compaction strains formed as a result of the applied pressure from the hot-press ram, pore pressure developed under resin melting, tooling constraints, and the temperature gradient in the part and the tool. The volumetric strain components E11, E22, and E33 computed for the 2D and 3D models are shown in Figure 8a and 8b. The volumetric strain component curves are seen split at the time pressure application began, which was much earlier in the 2D model than in the 3D model. Finally, the thickness

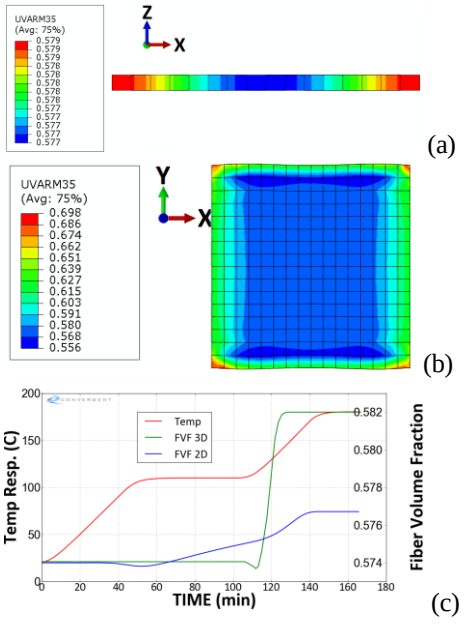

Figure 6: Fiber volume fraction (FVF) distribution in the (a) 2D model, (b) 3D model, and (c) FVF during the cure cycle analysis of the 2D and 3D models of panel.

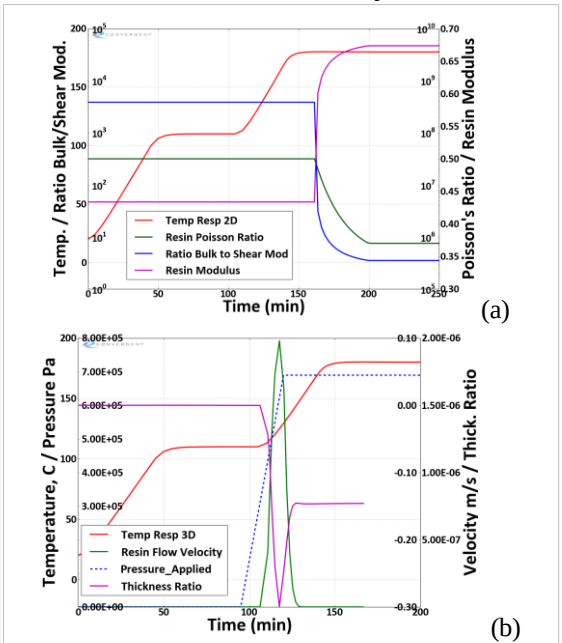

Figure 7: (a) Transition of mechanical properties in the 2D analysis, (b) thickness change during fiber-bed compaction in the 3D analysis of panel.

change in the 3D panel before and after compaction was computed as a ratio and plotted in Figure 7b, which is based on the difference in nodal displacements at the top and bottom surface. The thickness variation trends well with the viscosity, flow velocity, and pore pressure response variations (Figures 5d and 7b) due to applied temperature and pressure in the cure cycle.

Residual Strain Results During Curing and Upon Tool Removal

With known temperature distribution over the surface and known fiber volume fraction, the residual strain and warping analysis of the laminate was performed. The COMPRO® structural analysis is based on the instantaneous cure hardening approach [7], where resin is considered linearly elastic and modulus increases monotonically with degree of cure. The variation of the basic mechanical properties during the cure cycle as needed for the composite structural analysis such as ply modulus, Poisson's ratio, and thermal expansion coefficients were computed as a function of the temperature degree of cure and fiber volume fraction. The structural deformations, strains, and stresses were computed for the cure cycle. The forces at the interface of the part and the tooling assembly were released in the tool removal analysis, so that the composite part is free to deform as a rigid body. As a result of the rebalance of internal loads, the composite laminate deforms. The warping deformation computed from the 2D and 3D analysis are shown in Figure 9, for the $[0_{12}/90_{12}]$ cross-ply laminate having 0° plies along x axis (in the 2D and 3D

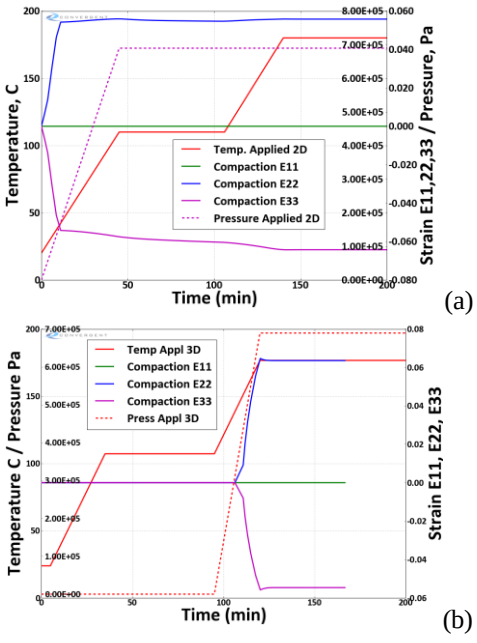

Figure 8: Fiber-bed compaction strains in the (a) 2D analysis, and (b) 3D analysis of panel.

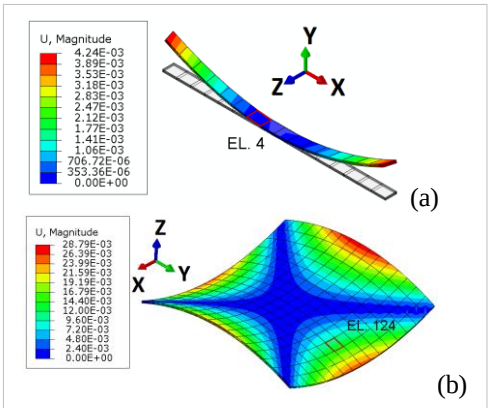

Figure 9: Warping deformation in (a) 2D and (b) 3D analysis of the $[0_{12}/90_{12}]$ panel.

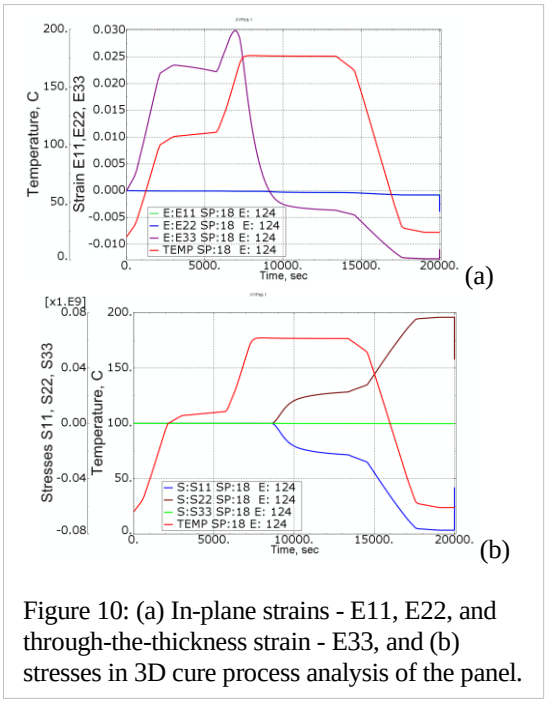

Figure 10: (a) In-plane strains - E11, E22, and through-the-thickness strain - E33, and (b) stresses in 3D cure process analysis of the panel.

models) and 90° plies along y axis (in the 3D model) or along z axis (in the 2D model). The 2D model could only capture the cross-sectional warping of the laminated panel, whereas the 3D model captured the complete deformation with double asymmetrical curvature on the panel edges.

The strains developed during the cure and upon tool removal in the 3D analysis are shown in Figure 10a, for the 18th ply, which is located in the 3rd element (no. 124) from the bottom surface. The corresponding strains from the 2D analysis are shown in Figure 11b, for the element 4 located at center of the strip. The through-the-thickness strains from the 2D analysis were comparable to those from the 3D analysis. In the 3D analysis, the in-plane strains E11 and E22, were compressive and an order of magnitude lower than the through-the-thickness strain E33 during the cure cycle. Other details of the in-plane strains from the 3D analysis will be discussed later. In the 2D analysis, the in-plane strains were smaller by a factor of 2 compared to those from the 3D analysis. In the tool removal time step (at 20,000 sec.), there was a rebalance of forces from the tool and the part, which caused a significant change in the in-plane strains E11 and E22 (Figure 10a), which is seen as a sudden jump in the strain curve. The in-plane stresses from the 3D analysis (Figure 10b) were comparable to those from 2D analysis (not plotted).

The cure shrinkage strain due to the chemical reaction in the resin occurred under applied heat flux, and the cure shrinkage strains from the 2D analysis are plotted in Figure 12. An estimate of the cure shrinkage strain was obtained, by separating the contributions from the cure shrinkage strains and the thermal expansion strains, by forcing expansion coefficients to be zero in the computation. This cure shrinkage strain was about 4%, and through-the-thickness strain was predominant among the three direct strains shown in the figure. Most of the cure shrinkage strain occurred in the time period from the middle of the second temperature ramp to the beginning of the temperature hold (Figure 12). The compressive cure shrinkage strain offsets the through-the-thickness tensile strain E33 (Figure 11b) to reduce the total strain during the temperature ramp up.

The significant variation in the through-the-thickness strain E33 (Figure 11b) came from the various contributing factors - (1) thermal expansion of the tool and the part during temperature ramps, (2) variation in thermal expansion coefficients

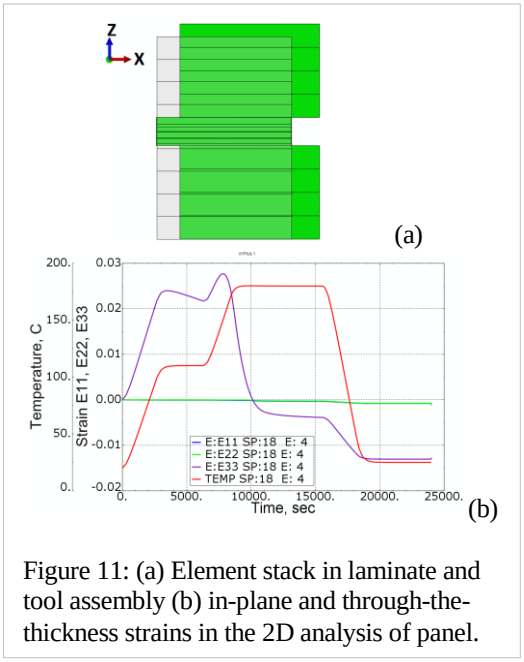

Figure 11: (a) Element stack in laminate and tool assembly (b) in-plane and through-the-thickness strains in the 2D analysis of panel.

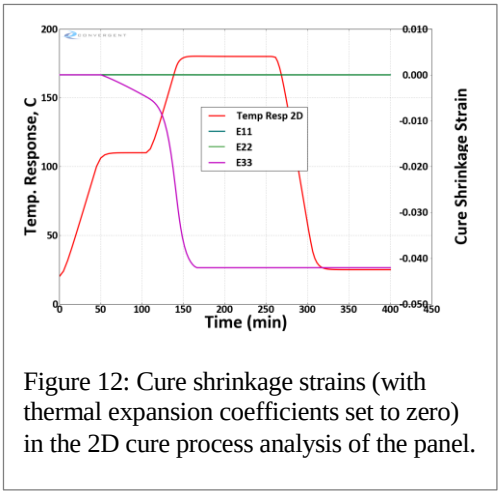

Figure 12: Cure shrinkage strains (with thermal expansion coefficients set to zero) in the 2D cure process analysis of the panel.

(a)

(b)

Figure 13: (a) Hot-press, and (b) hot-press chamber showing caul plate over prepreg and breather layers, and pressure rams (platens).

(CTE) of plies during cure, (3) rebalancing of applied pressure load with pore pressure development, and (4) resin cure shrinkage strain. The strain increase in the first 2500 sec. (42 min.) comes from the thermal expansion, and peak of this strain occurred between 6000 and 8000 sec. (100-133 min.). During the temperature ramps, the tool plate and the laminate expanded, both transversely and laterally. As a result, there was a significant lateral shearing of the laminate, as depicted in Figure 11a, which shows an instant of sheared cross-section of the laminate and tool. This shearing, coupled with contact friction forces, contributed to the through-the-thickness and in-plane strains. Further change in the through-the-thickness strain E33 occurred during the cool down cycle and upon tool removal. Moreover, there is coupling of the in-plane and out-of-plane deformations brought by the inherent asymmetry in the $0_{12}/90_{12}$ cross-ply panel. Additional results on the 3D model will be discussed after describing the test cases.

STRAIN MEASUREMENTS USING FIBER-OPTICS SENSORS

Several composite prepreg laminate configurations were fabricated in the hot-press (Figure 13). Hexcel® IM7-8552 unidirectional prepreg was cut into 30.5cm x 30.5cm (12in. x12in.) size sheets, and laid to the desired orientations to form a laminate stack of 24 plies. Both uniaxial and cross-ply layups of $[0_{12}/90_{12}]$ and $[+45_{12}/-45_{12}]$ plies were fabricated. The strain measurements were made during the curing of the laminated panels by means of optical fiber strain sensing techniques. The optical fiber containing fiber Bragg grating sensors (FBGs) were embedded between the resin impregnated prepreg sheets.

(a)

(b)

(c)

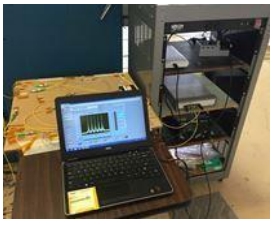

(d)

Figure 14: (a) Tunable laser optical system (TSL-710), (b) Agilent optical power meter, (c) sweep test system (SPU100), (d) data acquisition system software.

In the experimental setup, a tunable laser system, wavelength sweep system, and an optical

power meter were used to interrogate the spectral information from the embedded FBGs. A change in wavelength response from the FBGs provided a measure of strain at the embedded sensor location. The change of wavelength of an FBG due to strain and temperature can be approximately described by the equation (1), where, $\Delta\lambda$ is the wavelength shift and λ_o is the initial wavelength. The first term accounts for impact of

$$\frac{\Delta\lambda}{\lambda_0} = (1-p_e)\varepsilon + (\alpha_\Lambda + \alpha_n)\Delta T \qquad (1)$$

strain on the wavelength shift, ε is the strain experienced by the grating, where p_e is 0.24 as specified by the FBG manufacturer. The second term accounts for the temperature effects on the wavelength shift, where α_Λ is the thermal expansion coefficient and α_n is the thermo-optic coefficient. The coefficient specified for $(\alpha_\Lambda + \alpha_n)$ is 7.5×10^{-6}.

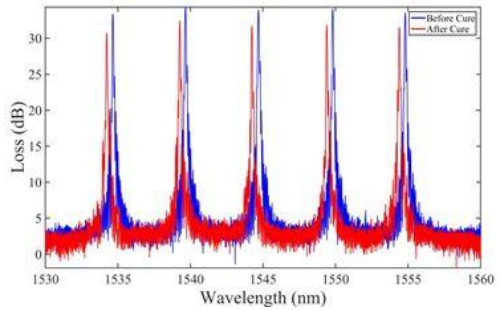

Figure 15: Optical signal power loss v/s wavelength before and after cure & tool removal.

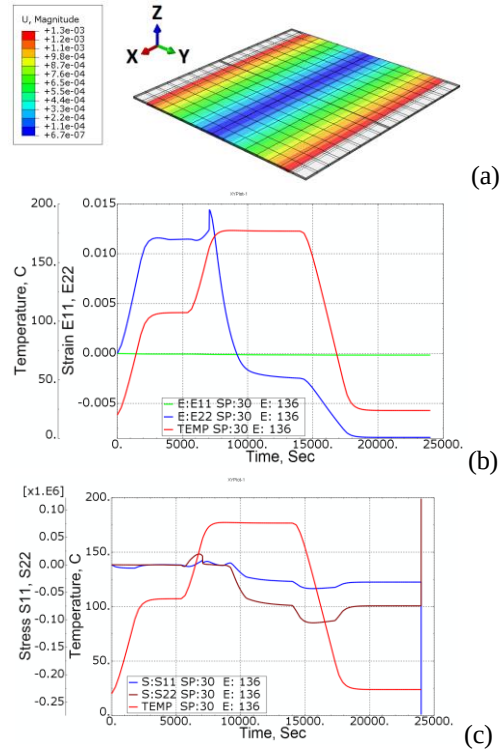

Figure 16: (a) Deformation in uniaxial panel; (b) residual strains (in-plane) and (c) residual stresses, during curing and upon tool removal.

A Santec tunable laser (TSL-710, Figure 14a) was used to create a narrow-band light wave at a specified wavelength. The light wave is passed to the FBGs through a passive optical circulator, which functions to direct the wave from one port to another in a single direction. Reflected light from the FBG travels back through the optical circulator into the Agilent optical power meter (Figure 14b). The optical power meter measures the wavelength dependent loss, which is a ratio of the power of the reflected light to the power of a reference signal through an optical fiber without FBGs. The wavelength of the emitted light wave is swept across a specified wavelength range, (for example, 1530 to 1560 nm, Figure 15) using a swept processing unit SPU-100 (Figure 14c). When the wavelength of the tunable laser matches the Bragg wavelength of the FBG, the optical power meter sees the maximum wavelength dependent loss (Figure 15). The wavelength at which this response occurs corresponds to the temperature and/or strain of the FBG. The sweeping process is repeated through the cure cycle. The complete Swept Test System combines a Santec tunable lasers (TSL-710) with an Agilent optical power meter (N7744A) and Swept Processing Unit (SPU-100). The optical power meter has four optical channels that are simultaneously sampled for measurement of FBG strain. All scans of the sampled

data are automatically parsed into individual sensor measurements for scaling the data into appropriate engineering units. The post-processing of data is all accomplished using a MATLAB software.

An optical fiber with five FBG sensors was embedded at the 18th ply from the bottom of the panel, equidistant from the side edges of the panel. Strain measurements from the FBGs were made in real-time during curing and data were recorded continuously at defined time intervals.

Temperature measurements were made with thermo-couples embedded inside the laminate. Five thermo-couples were embedded in the laminate at locations near the FBGs, with sufficient offset from the FBGs so as not to affect the optical signals. Three thermo-couples were placed outside the panel, along the outer edge of the panel that is surrounded by the tooling assembly of the hot-press (Figure 13b). A National Instrument (NI) data acquisition system was used with NI Express software.

RESIDUAL STRAIN ANALYSIS OF EXPERIMENTAL TEST CASES

The results from the cure process analysis simulations of the experimental test cases performed are summarized here. The residual strain responses from the uniaxial laminate shows significant transverse compressive strains E22 (Figure 16b) and strain E33 (not shown; ~ E22) normal to the fiber direction (x axis). The large strains during temperature ramp up are due to the development of a higher thermal expansion coefficient (CTE) which is a function of degree of cure and temperature, and other factors as discussed above. Also, the resin cure shrinkage is much larger in the lateral

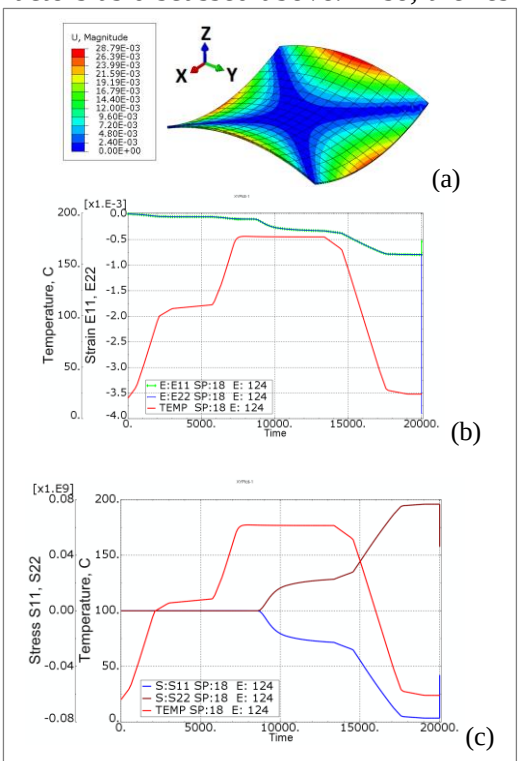

Figure 17: Warping deformation in [0_{12}/90_{12}] cross-ply panel; (b) residual strains (in-plane), and (c) residual stresses, during curing and upon tool removal.

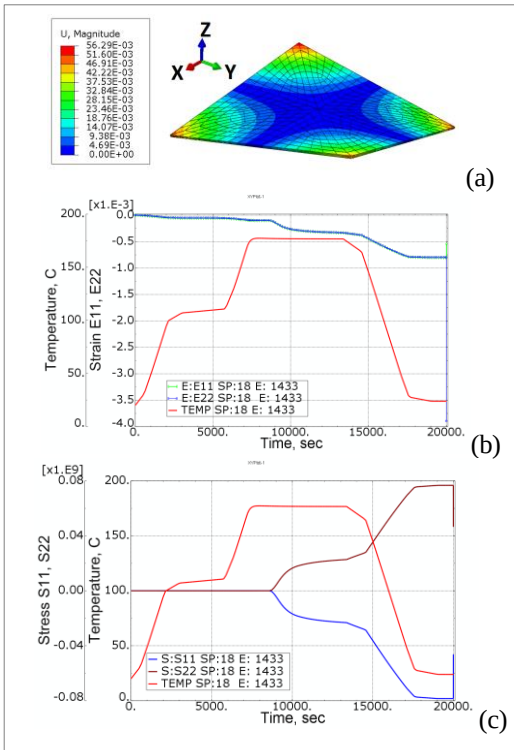

Figure 18: Warping deformation in [+45_{12} /-45_{12}] cross-ply panel; (b) residual strains (in-plane), and (c) residual stresses, during curing and upon tool removal.

direction (y axis) than in the fiber direction. No warpage is seen in the uniaxial laminate, since there is no bending. The residual stresses, shown in Figure 16c, were small. The compressive lateral strain from the analysis was 8,000 micro strains upon tool removal (24,000 sec.).

The residual strains E11, E22 upon curing of the $[0_{12}/90_{12}]$ laminate, which were discussed previously, are plotted in the Figure 17b. These strains are an order of magnitude smaller than E33 (Fig. 10a), unlike those in the uniaxial case, where E22, and E33 were of the same order of magnitude. The cured panel shows considerable warping (Figure 17a) with double curvature on the panel edges.

The residual strains in the $[45_{12}/-45_{12}]$ laminate curing case are plotted in Figure 18b, along with the warping deformation. Considerable unsymmetrical warping is seen at the panel corner, with two opposite corners deformed upward, and the other two corners downward. The magnitude of the deformation in this case is nearly double that of the 0/90 case, since corners are less stiff here. The in-plane residual strains and stresses were about the same as in the 0/90 case.

COMPARISON OF RESIDUAL STRAINS FROM ANALYSIS AND EXPERIMENTAL TESTS

A preliminary comparison of the residual strains from the analysis and test was made on the three laminate cases – a uniaxial case, and two cross-ply, 0/90 and +45/-45, cases. The residual strains measured from an embedded FBG sensor along with those computed from analysis are plotted in Figures 19-21. Photographs of the cured panels are shown in Figure 22. The residual strains measured from all five FBGs had similar trends with some differences in amplitudes, and hence were not plotted for clarity in these figures. The applied and response temperatures from the analysis and test during the cure cycle are plotted in the figures. Temperature response from the heat-transfer analysis generally compared well with those

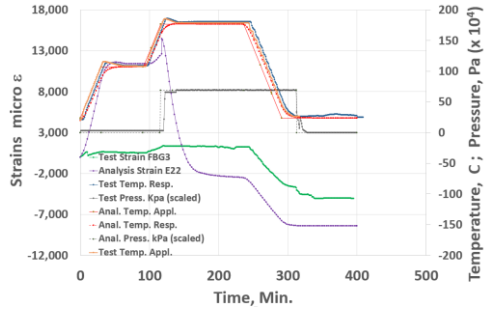

Figure 19: Comparison of measured and analysis strain during curing, and residual strain of the uniaxial laminate.

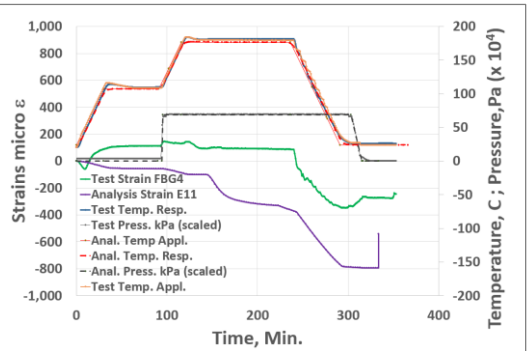

Figure 20: Comparison of measured and analysis strain during curing, and residual strain of the 0/90° cross-ply laminate.

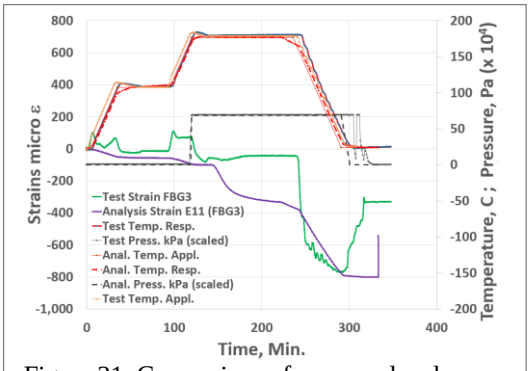

Figure 21: Comparison of measured and analysis strain during curing, and residual strain of the 45/-45° cross-ply laminate.

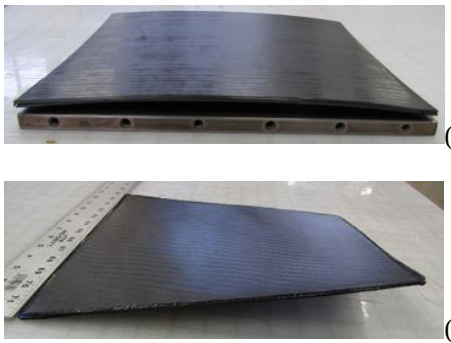

Figure 22: Warpage in unbalanced cross-ply laminates (a) 0/90°, and (b) +45/-45°

measured using thermo-couples. The temperature overshoot after the second ramp was due to hot press temperature control system enforcing applied temperature on the part, and is not the exothermal peak of reaction.

In the cross-ply laminate cases, the FBGs were placed along the fiber direction. The FBGs were placed at the 18th ply from the bottom of the panel. In the uniaxial case, the FBGs were placed normal to the fiber direction, in a slit cut in the middle 6 prepreg sheets so that fibers did not overlap the FBGs, to minimize errors in measured strain when the fibers bend over the sensor wire of larger diameter.

The residual strain curves plotted from the analysis and test results show that they have a similar overall trend during the curing cycle. However, in the uniaxial case, during the temperature ramp up, the residual strains from the analysis were significantly large compared to test strains. In the uniaxial case, the residual strain that remained after tool removal was about ~5050 micro strains in the test verses ~8000 in the analysis, which are attributed to the resin contraction under cooling and resin cure shrinkage. Reference [12] notes a residual strain of 4200 micro strain was measured in a 24 ply uniaxial graphite epoxy laminate cured at 130° C. Also, reference [13], notes a strain of 4960 micro strain at the end of curing of a pure epoxy of Bisphenol A-type EP at 170° C. The measured strain appear to be consistent with those noted in the references [12, 13], although these cases are not directly comparable.

At this time, there was little indication on the exact causes for the variation between the analysis and test strain. However, a few plausible factors that might have caused the differences between the measured strain and predicted strain are indicated here. Factors related to the analysis data include - high values of the resin modulus corresponding to the low viscosity state, in the early stage of cure, causing significant strain build up during the temperature ramp up in the uniaxial case; the lack of available open source Hexcel® 8552 data on the resin modulus characteristics; coupling of in-plane and high shear strains arising in the contact mechanism of the part and tool assembly of the hot-press cure; and omitted contribution of compaction strains in the total-strain.

Factors related to test include - slippage in the embedded FBG's preventing accurate strain measurements in the low viscosity state of the resin during the heating cycle; slit cut across to embed FBGs normal to the fiber in the uniaxial case, which could have prevented bonding of the optical sensor with adjacent material until the resin solidified in the cure; and unverified coefficients to factor out FBG strain and temperature components from the wavelength data of the FBGs.

Residual strain results from the test and analysis on the cure process of 0/90 cross-ply laminate are plotted in Figure 20. In this case, the residual strains measured with FBG4 located at 0.1m from the panel edge were compared with the analysis strains at element 124 (Figure 9b). The resulting analysis and test strain trends compare well during the cure cycle, as well as during the tool-removal step, although the magnitudes differed. Nevertheless, the magnitude of strain during temperature ramp up were much

less than those in the uniaxial case, because stiffer cross-fibers helped to absorb the axial strains developed. The magnitude of the residual strain after cooling and tool removal are ~-250 micro strain in the test versus ~-450 micro strain in the analysis. The measured strains appear to be consistent with those noted in reference [14], where residual strains of -440 micro strain were measured in a 24 ply 0/90° cross ply laminate CU-125 NS GR/EP prepreg material. Both the test and analysis simulations presented a significant anti-symmetric warping deformation with two opposite edges having curvature bowing down, and other set of edges bowing up (Figures 20, 22).

Figure 21 shows the residual strain results from the analysis and test of 45/-45° cross-ply laminate at the center location of the panel. Again, the FBGs are placed in the fiber direction at the 18th ply location from the bottom. The strains from the test and the analysis trended well and the magnitude appears to be matching well for the temperature ramp up phase and the cool down phase of the cure cycle. The magnitude of the residual strain after cooling and tool removal are -300 micro strain in the test versus -500 micro strain in the analysis, and are of the same order of magnitude as in the 0/90° laminate case. However, the maximum magnitude of warping deformation in the 45/-45° case is double that of the 0/90° case (Figures 17a, 18a). The warping from both the analysis and test are asymmetrical with peak deformation at the corners (Figures 21, and 22)

CONCLUDING REMARKS

Composite cure process induced residual strains and warping presents significant challenges in manufacturing. Cure process models of composite laminates were developed to analyze and understand the laminate cure responses with reference to the known physics of the composite curing process, and to compare the residual strain predictions from the analysis with those measured using fiber optics strain sensors in the laboratory test. Analytical studies involved thermo-kinetic response, resin flow compaction response, and structural response analysis. The cure process responses were simulated using COMPRO®/RAVEN® software and associated material characteristics available in its material database.

The results from the thermo-chemical, flow-compaction and structural analysis on the 2D and 3D models were presented, compared, and discussed with reference to the formation of residual strains, and warping deformations. Residual strain measurement results from the experimental tests with embedded fiber optic strain sensors, were presented, and compared with cure process analysis results.

A significant understanding of the multitude of spatial and temporal variables affecting the thermo-chemical responses, flow-compaction responses, and residual strain responses were obtained in this study. Particular findings are the following:

1. Many cure process response results from the simulation were traced to the known physical phenomenon occurring in the cure such as cure kinetics, chemical shrinkage, viscous behavior, resin flow in porous media, fiber-bed compaction, thermal expansions, contact friction, and material elasticity.
2. Primary material characteristics of the Hexcel® 8552 resin, such as degree of cure, viscosity, resin modulus and their effect on intermediate cure responses such as pore pressure, flow velocity, fiber volume fraction, compaction and shrinkage strains that lead to the formation of total strain responses were explored in the three laminate configurations studied.

3. During the heating cycle, large tensile strains E22, and E33 predicted in the uniaxial laminate analysis were not captured in the test, and plausible factors to trace these differences such as modulus, slippage of FBGs were identified.
4. Strain trends from the cross-ply laminate analysis mostly agreed with the test as discussed previously, indicating the capability of the physics based cure process models in predicting the residual strains.

In conclusion, this analytical and experimental study has provided insight into bridging the gap between the known physics of the cure process and the use of cure process simulation software and optical strain measurement techniques to understand the development of residual strain responses in the curing of laminates in a hot press.

ACKNOWLEDGEMENT

The authors gratefully acknowledge technical discussions on the COMPRO® and RAVEN® software with Mr. C. Lynam, Dr. A. Forghani, and Dr. A. Arafath, from the Convergent Manufacturing Technology (CMT), Vancouver, BC, Canada.

REFERENCES

1. Lee, W.L., Loos, A.C., and Springer, G.S., "Heat of Reaction, Degree of Cure, and Viscosity of Hercules 3501-6 Resin," Journal of Composite Materials, Vol. 16, Nov. 1982.
2. Loos, A. C., and Springer, G.S., "Curing of Epoxy Matrix Composites," Journal of Composite Materials, Vol. 17, March 1983.
3. Kim, K.S., and Hahn, H.T., "Residual Stress Development during Processing of Graphite/Epoxy Composites", Composites Science and Technology, Vol. 36, pp. 121-132, 1989.
4. White, S.R., and Han, H.T, "Process Modeling of Composite Materials: Residual Stress Development during cure. Part I. Model Formulation,"; "…Part II. Experimental Validation," Journal of Composite Materials, Vol. 26, No. 16, 1992.
5. Bogetti, T.A., and Gillespie, J.W., "Process-Induced Stress and Deformation in Thick-Section Thermoset Composite Laminates," Journal of Composite Materials Vol. 26, No. 5, pp. 626-660, 1992.
6. Smith, G.D., and Poursartip, A.,"A Comparison of Two Resin Flow Models for Laminate Processing," J. of Composite Materials, Vol. 27, No. 17, 1993.
7. Johnston, A., Vaziri, R., and Poursartip, A., "A Plane Strain Model for Process-Induced Deformation of Laminated Composite Structures," Journal of Composite Materials, Vol. 35, No. 16, 2001.
8. Hubert, P., and Poursartip, A., "Aspects of the Compaction of Composite Angle Laminates: An Experimental Investigation," Journal of Composite Materials, Vol. 35, No. 1, 2001.
9. COMPRO Common Component Architecture User's Guide, Release 2.0, Convergent Manufacturing Technologies Inc., Vancouver BC, Canada, August 12, 2008.
10. Introduction to COMPRO; Introduction to RAVEN; COMPRO Model Documentation, Convergent Manufacturing Technologies Inc., Vancouver BC, Canada, 2014.
11. ABAQUS, The Abaqus software is a product of Dassault Systèmes Simulia Corp., Providence, RI, USA, 2013.
12. Kang H., Kang D., et al., "Cure Monitoring of Composite Laminates using Fiber Optic Sensors," Smart Materials and Structures, Vol. 11, pp 279–287, 2002.
13. M. Harsch, et al., "Influence of Cure Regime on the Strain Development in an Epoxy Resin as Monitored by a Fiber Bragg Grating Sensor," Macromol. Mater. Eng., Vol. 292, pp. 474–483, 2007.
14. Kang H., Kang D., et al., "Simultaneous Monitoring of Strain and Temperature during and after Cure of Unsymmetric Composite Laminate using Fibre-Optic Sensors," Smart Materials and Structures, Vol. 12, pp 29–35, 2003.